**Proceedings of the 36th International Conference on Ocean, Offshore & Arctic Engineering**
**OMAE2017**
**June 25-30, 2017, Trondheim, Norway**

# OMAE2017-61415

## PROTOTYPE REYNOLDS NUMBER VIV TESTS ON A FULL-SCALE RIGID RISER

**Decao Yin**
SINTEF Ocean [1]
**Trondheim, Norway**

**Halvor Lie**
SINTEF Ocean [1]
**Trondheim, Norway**

**Rolf J. Baarholm**
STATOIL
**Stjørdal, Norway**

### ABSTRACT

Slender offshore structures in deep water subjected to currents may experience vortex-induced vibrations (VIV), which can cause significant fatigue damage. Extensive experimental researches have been conducted to study the VIV in the past several decades. However, most of the experimental works have small-scale models and relatively low Reynolds number (Re) – 'subcritical' or even lower Reynolds number regime. There is a lack of full understanding the VIV in prototype Re flow regime. Applying the results with low Re to a full scale riser with prototype Re might have uncertainties due to the scaling effects. In addition, the surface roughness of the riser is also an important parameter, especially in prototype Re regime.

In present study, two full-scale rigid riser models with different surface roughness ratios were tested in the towing tank of MARINTEK in 2014. Stationary tests, pure cross-flow (CF) free oscillation tests and forced/controlled motion tests were carried out.

Several conclusions could be made:

- The drag coefficient is dependent on the Re number and surface roughness ratio.
- At critical and supercritical flow regimes, the displacement amplitude ratio is less sensitive to Re than that at lower Re. The displacement amplitude ratio in subcritical flow regime is significantly larger than that in critical and supercritical flow regimes.
- Two excitation regions for the 'smooth riser' and one excitation region for the 'rough riser' are identified.

### INTRODUCTION

A literature review on the effects of Reynolds number ($Re = UD/\nu$) and surface roughness ratio on the VIV responses were done by [1]. The drag coefficient, maximum response amplitude, Strouhal number and excitation coefficients are strongly depending on Re and surface roughness in the critical and post-critical flow regime, indicating that these effects should be accounted for in future VIV analysis. A 'scaling' method on the excitation coefficients was introduced to account for various Reynolds number and surface roughness.

Several studies investigated the Reynolds number effects on the peak CF amplitude ratio of a freely oscillating rigid circular cylinder [2] [3]. By studying experimental results, both studies demonstrated that the peak CF amplitude ratio depend on the Reynolds number and damping. However, mainly due to the limit of experimental setup, the Reynolds number ranges are $525 - 2600$ in [2] and $500 - 33000$ in [3] respectively, both are in the subcritical flow regime. In addition, the surface roughness effect on the response amplitude was not studied.

Response of flexible pipes were reviewed by [4], the Reynolds number ranges from $10^3$ to $2\times10^5$, it was found that the response amplitude increases with increased Reynolds number. [5] studied Shell flexible pipe VIV model tests, which was carried out at MARINTEK's Ocean Basin. The Reynolds number range is roughly $5\times10^3 - 2.2\times10^5$. The Reynolds number effect on the response found by [4] was confirmed, the influence of surface roughness ratio is also mentioned in [5]. The influential parameters on the responses have similarities between a flexible pipe and a freely oscillating rigid cylinder.

There are few experimental studies on VIV at prototype Reynolds number ($>10^5$), mainly due to the limitation of the test facilities. ExxonMobil performed full scale Re number VIV model tests on rigid bare riser and riser with helical strakes, the Reynolds number ranges from $8\times10^4$ to more than $10^6$ [6]. Various surface roughnesses were modelled by using sandpaper. It was found that in critical Reynolds number regime, the VIV response amplitude and the excitation coefficient of a bare riser are sensitive to Reynolds number and surface roughness. In Deepstar high Reynolds number experiments, combined in-line (IL) and CF VIV experiments were carried out at a Reynolds number range from $3.1\times10^5$ to $7.1\times10^5$ [7]. A rough cylinder was tested, desired roughness was achieved by fit a fiberglass sleeve outside the smooth cylinder, and covered in sand particles, the surface roughness ratio $k/D = 2.3\times10^{-3}$ [7]. 'Dual resonance' was observed for both subcritical smooth cylinder

[1] Earlier MARINTEK, SINTEF Ocean from 1st January 2017 through a merger internally in the SINTEF Group

tests and supercritical rough cylinder tests when IL motion is allowed. Large 3rd order harmonic lift force components were measured at prototype Reynolds number. Stable 'figure 8' response orbits were observed at supercritical Re tests.

To fill the knowledge gap of VIV at prototype Re and overcome shortage of applying results at lower Re to prototype Re, a new innovative VIV test rig was designed and built at MARINTEK to test a full-scale rigid riser model. This test rig was first used to study possible VIV suppression to improve operability of retrievable riser systems with auxiliary lines by adding riser fins, the model tests were carried out during 2011/2012 [8]. In MARINTEK's very first prototype Re VIV tests on a full scale riser section [8], distinct difference of response amplitude ratios were observed between 'critical' and 'sub-critical' Re flow regimes, the largest amplitude ratio in 'critical' Re is around 60% of that in 'sub-critical' Re.

## NOMENCLATURE

| | |
|---|---|
| $A_{nom}/D$ | Nominal amplitude ratio |
| $A^*$ | Peak/maximum amplitude ratio |
| $C_D$ | Drag coefficient |
| $C_e$ | Excitation coefficient |
| $D$ | Outer diameter of the riser model |
| CF | Cross-flow |
| $F_h$ | Hydrodynamic force |
| $F_{h0}$ | Amplitude of harmonic hydrodynamic force |
| $F_m$ | Measured force in forced motion test |
| $f_{osc}$ | Oscillation frequency |
| $f_v$ | Vortex shedding frequency |
| $\hat{f} = \frac{f_{osc}D}{U}$ | Non-dimensional oscillation frequency |
| IL | In-line |
| $k/D$ | Roughness ratio |
| $L$ | Length of the riser model |
| $m^*$ | Mass ratio |
| NDP | Norwgian Deepwater Programme |
| OQUS | Optical tracking system |
| Re | Reynolds number |
| $St$ | Strouhal number |
| $T_n$ | Natural period |
| $U$ | Current velocity |
| $U_r = \frac{UT_n}{D}$ | Reduced velocity |
| VIV | Vortex-induced vibrations |
| $\Delta l$ | Distance between measurement stations |
| $\Delta M$ | Bending moment difference |
| $\sigma_{CF}$ | Standard deviation of CF motion |
| $\nu$ | Kinematic viscosity |
| $\rho$ | Density of the fluid |
| $\varphi$ | Phase angle between CF motion and hydrodynamic force |
| $\zeta$ | Damping ratio |

## THEORETICAL BACKGROUND

A brief introduction of the governing equation of motion of a freely oscillating circular cylinder in y-direction (CF) is:

$$m\ddot{y} + c\dot{y} + ky = F_h \tag{1}$$

where $m$ is total oscillating structural mass, $c$ is structural damping, $k$ is stiffness, $F_h$ is hydrodynamic force in CF direction.

Some of the dimensionless parameters of equation (1):
Mass ratio

$$m^* = \frac{m}{\frac{1}{4}\pi\rho D^2 L} \tag{2}$$

Damping ratio

$$\zeta = \frac{c}{2\sqrt{k(m+m_a)}} \tag{3}$$

where $m_a$ is the added mass.
Reduced velocity

$$U_r = UT_n/D \tag{4}$$

where $T_n$ is the natural period.
If the CF displacement is harmonic, it can be described by

$$y(t) = y_0 sin(\omega_{osc} t) \tag{5}$$

where $\omega_{osc} = 2\pi f_{osc}$; $f_{osc}$ is oscillation frequency.

The hydrodynamic force is reasonably represented by

$$F_h(t) = F_{h0} sin(\omega_{osc} t + \varphi) \tag{6}$$

where $\varphi$ is the phase angle between the CF motion and hydrodynamic force.

For a circular cylinder undergoing forced motion, equation (1) becomes

$$m\ddot{y} - F_h = F_m \tag{7}$$

where $F_m$ is measured force.

The following non-dimensional coefficients are discussed in this paper:

The drag coefficient is defined by

$$C_D = \frac{\bar{F}_{IL}}{\frac{1}{2}\rho DLU^2} \tag{8}$$

where $\bar{F}_{IL}$ is the mean force in IL direction.

The dynamic excitation coefficient at oscillation frequency $\omega_{osc}$ is defined as [9]:

$$C_e = \frac{4}{\rho DLU^2 \omega_{osc} y_0} \lim_{k\to\infty} \frac{\int_t^{t+kT} F_h(\tau)\cdot\dot{y}(\tau)d\tau}{kT} \tag{9}$$

where $\dot{y}(t)$ is the oscillation velocity in CF direction.

This force coefficient defines the energy transfer between fluid and cylinder for each harmonic component present in the time series. Positive value means that energy is transferred from the fluid to the cylinder, while a negative coefficient indicates energy dissipation through hydrodynamic damping.

## TEST SET-UP

The model tests were performed in Towing Tanks I+III at MARINTEK. The water depth of Tank I is 5.6 m and 10 m for Tank III. The total length is 260 m, and it is 10.5 m wide. The towing tank is equipped with an overhead towing carriage, which can run along the tank in both directions.

During tests, a full scale VIV test rig was hinged to the carriage. The test rig was manufactured by MARINTEK to test prototype riser models, and first used by [8]. A principle sketch of the test rig is shown in Figure 1. A photo with the test rig and the smooth riser model is shown in Figure 2. The test rig comprises three vertical steel truss works, hinged together in a U-shape. The full scale riser model with an outer diameter of 0.533 m was mounted onto the test rig vertically and submerged in water. Two end-plates with a diameter of 2 m were fitted at both ends of the riser model, so that the boundary effects from water surface and bottom of the tank could be mitigated, and the flow over the test riser section was close to two dimensional.

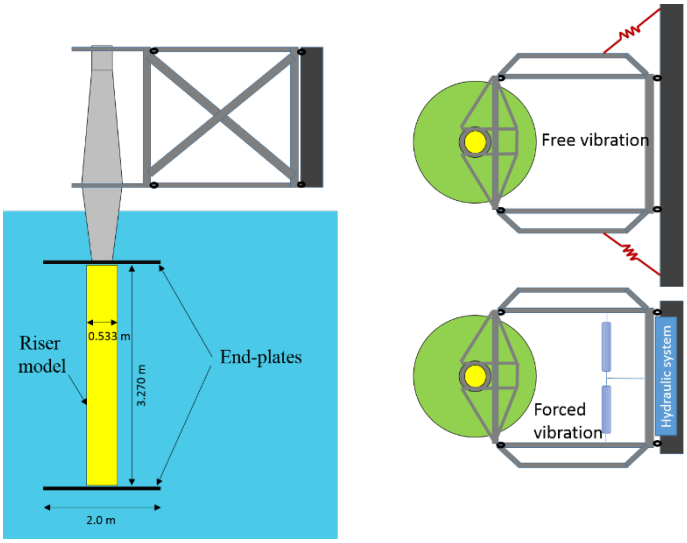


**Figure 1 Principle sketch of MARINTEK's full scale VIV test rig. Left: Side view. Upper right: Top view of free vibration set-up. Lower right: Top view of forced vibration set-up.**

The hinged test rig enables the tested riser model to move in a semi-arc path. Since the radius of this 'semi-arc' path is 5 m, which is much larger than the expected CF oscillation amplitude, the resulted IL motion can be neglected. So we assume present VIV tests have pure CF motions.

For free oscillation VIV tests, the test rig was elastically mounted by use of tension coil springs to obtain a desired natural period $T_n$.

In [8], one spring setup was used for all the free oscillation tests, so the system has the same natural oscillation frequency in water. To achieve different reduced velocities, the towing speed was varied, and so the Re. In present tests, the Re was kept the same, we tuned the natural oscillation period to achieve desired reduced velocity. Three sets of tension coil springs were deployed and mounted in certain ways in order to get wanted natural periods.

Forced motion test was also conducted in a later phase. In these tests, the spring system was replaced by a hydraulic system, desired oscillation amplitude and frequency were input to the control system and achieved by the hydraulic cylinders.

The entire system was towed by the carriage through calm water to simulate uniform current past on the riser section.

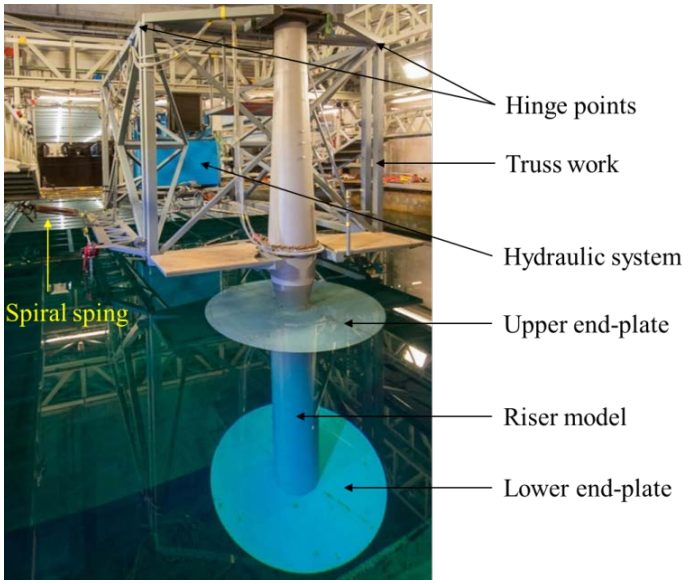


**Figure 2 Photo of the test rig with smooth riser model.**

## RISER MODELS

Two steel pipes were manufactured to model full scale riser sections. One was painted to have a smooth outer surface, and the other was wrapped with P36 sandpaper to model rough outer surface due to marine growth (see Figure 3). The key properties of the riser models are shown in Table 1.

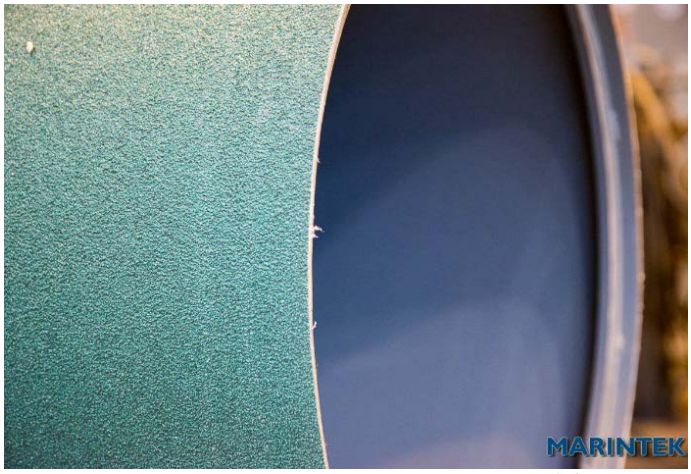


**Figure 3 Rough surface modelled by sandpaper, $k/D = 1.0 \times 10^{-3}$.**

**Table 1 Key properties of the riser model.**

| Property | Unit | Value |
|---|---|---|
| Length of the riser model, $L$ | m | 3.270 |
| Outer diameter, $D$ | m | 0.533 |
| Thickness | m | 0.002 |
| $k/D$ of smooth riser model | - | 5.3e-5 |
| $k/D$ of rough riser model | - | 1.0e-3 |

## INSTRUMENTATION

The following instrumentations/measurements are included:

- The standard measuring equipment on the towing carriage measured towing speed.
- In [8], the forces acting on the test riser model were measured by use of an assembled set of one-component force transducers, which were mounted on the riser model end.

  In present model tests, a central core beam was manufactured and equipped with strain gauge force transducers, which measured the bending moments at four stations of the inner core beam.

  The tested riser model was fastened to the inner core beam at two connection points in the middle of the riser section. Except for that, there was no other contact between the riser model and inner core beam. There were also gaps between the riser model and two end-plates.

  The basic principle is to use difference of bending moments to derive force: $F = \Delta M/\Delta l$. By using the measured bending moments at Station 3 and Station 4, the force acting on the lower end-plate was calculated. In the same way, the force acting on the riser model was found and further processed.
- The riser oscillation displacement was measured by an optical tracking system (OQUS); in addition, a potentiometer measured the rig oscillations.
- A three-component accelerometer was located at topside of the rig on the 'cone-shape' support structure. Measured accelerations were used to document vibrations in the test rig.

All the transducer signals were sampled at 1200 Hz except the OQUS, which has a sampling frequency of 25 Hz. The low-pass analogue filtering cutoff frequency was 250 Hz. Calm water condition for each test run was assured by waiting at least 10 minutes between tests.

## TEST PROGRAM

The following tests were carried out:

- Instrumentation verification and calibration tests
- Decay tests and pluck tests in air and still water
- Stationary tests
- Pure CF free oscillation tests
- Pure CF forced oscillation tests

Decay tests were performed in air on the test rig without riser model, in order to investigate the structural damping of the test rig. The damping ratio was found to be between 1-2%. Figure 4 shows the time history of displacement at the riser location of one decay test in air.

Decay tests were also performed in still water for each spring set, before free oscillation test. The natural frequencies in water and the damping ratio were measured for each decay test in water. Figure 5 shows the time history of displacement at the riser location of one decay test in water, the damping ratio was 3.6%.

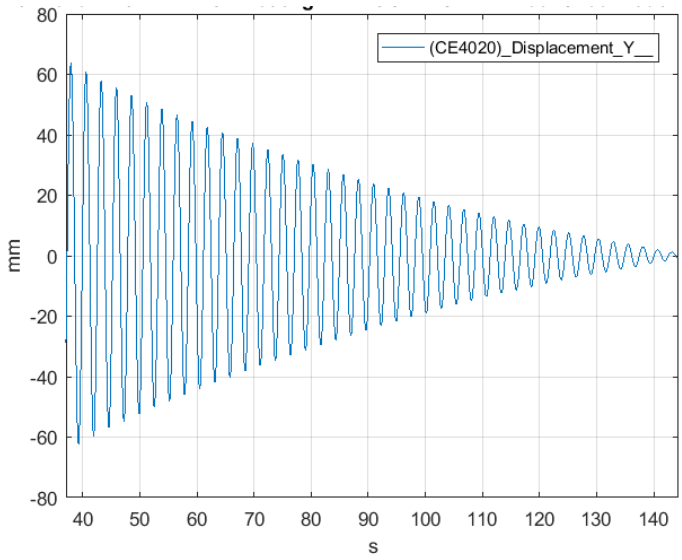


**Figure 4 Decay test in air, without riser model, $T_n$=2.62 s, damping ratio is 1.3%.**

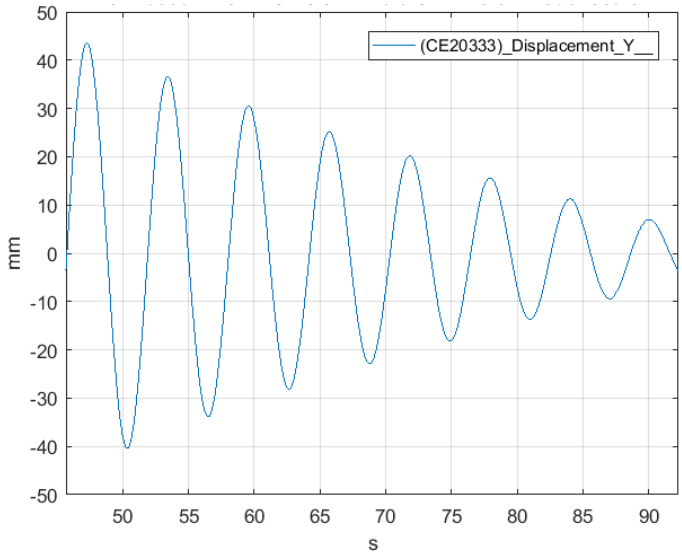


**Figure 5 Decay test in water, with smooth riser model, $T_n$=5.82 s, damping ratio is 3.6%.**

Stationary tests were performed on both fixed smooth and rough riser models, at the Re range from subcritical to critical regimes.

Free oscillation tests were performed on both smooth and rough riser models, at selected critical Re and a range of reduced velocities. In addition, some tests in [8] were repeated with varying Re. The test program of stationary and free oscillation tests is shown in Table 2.

Forced motion tests were carried out at $\mathrm{Re} = 4{\times}10^5$, on both smooth and rough riser models. The test matrix with varying amplitude ratios ($A/D$) and non-dimensional oscillation frequencies ($\hat{f} = f_{osc}D/U$) is presented in Figure 6. The purpose of these tests was to establish prototype Re hydrodynamic force coefficient database which can be further used by VIV analysis programs such as VIVANA [10].

**Table 2 Test program of stationary and free oscillation tests.**

| | $k/D$ | Re | $U_r$ |
|---|---|---|---|
| Stationary tests | 5.3e-5 | 9e4 - 8e5 | - |
| | 1.0e-3 | 9e4 - 6e5 | - |
| Free oscillation tests | 5.3e-5 | 1e5 - 2.6e5 | 5 - 12 |
| | | 3e5 | 4 - 10 |
| | | 4e5 | 5 - 13 |
| | | 6e5 | 5 - 11 |
| | 1.0e-3 | 2.5e5 - 3.5e5 | 7 - 11 |
| | | 2e5 | 4 - 8 |
| | | 4e5 | 8 - 12 |

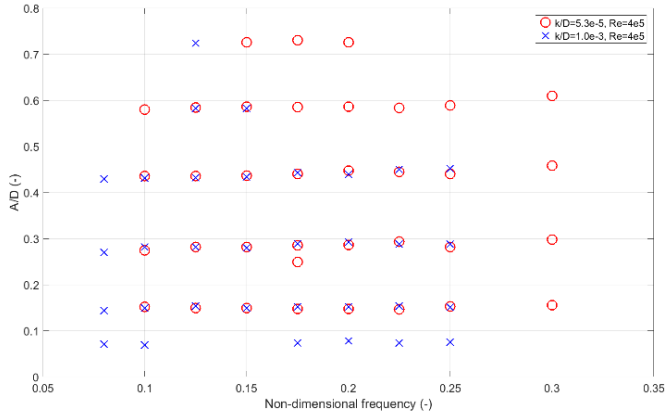


**Figure 6 Test matrix of forced motion tests.**

## RESULTS

### Drag coefficient

Drag coefficient of both smooth and rough circular cylinders are presented in Figure 7 as results from the stationary tests. The effects of the surface roughness ratio on the drag coefficient is clearly seen. 'Drag crisis' is a phenomenon that drag coefficient decreases abruptly as Reynolds number increases. Simultaneously, the boundary layer flow around the bluff body transits from laminar to turbulent [11]. The rough cylinder has 'drag crisis' at $\mathrm{Re} = 1.26{\times}10^5$, while the smooth cylinder has the 'drag crisis' at $\mathrm{Re} = 2.98{\times}10^5$. And the lowest drag coefficient of the rough cylinder (0.44) is larger than that of smooth cylinder (0.36). This is consistent with existing literatures [1]. Due to roughness at the cylinder surface, the transition of the boundary layer from laminar to turbulent occurs at lower Reynolds numbers. Consequently, the critical and supercritical flow regimes shift to lower Reynolds numbers [12]. When the surface roughness ratio is larger than a critical value, the 'drag crisis' disappears accordingly [13][14].

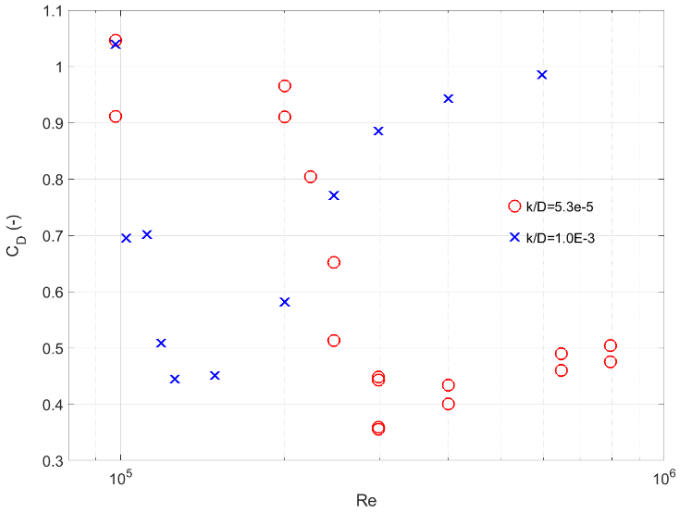


**Figure 7 Drag coefficients from stationary tests.**

### Strouhal number

Spectral analysis has been performed on the CF force of stationary tests, the peak frequencies correspond to the vortex shedding frequency $f_v$. It is well known that the Strouhal number is defined as $St = f_v D/U$, calculated Strouhal number is shown in Figure 8.

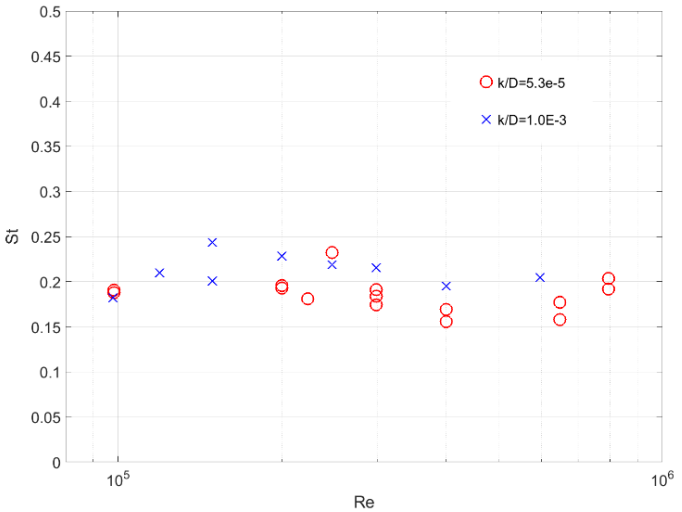


**Figure 8 Strouhal number from stationary tests.**

It shows that when Re is in the range $9 \times 10^4$ - $8 \times 10^5$, the *St* of both cylinders is between 0.15 and 0.25. The *St* at Re from $3 \times 10^5$ to $8 \times 10^5$ is slightly lower than the *St* at Re from $1 \times 10^5$ to $3 \times 10^5$. The rough cylinder ($k/D = 1.0 \times$

$10^{-3}$) has relative higher *St* than the smooth cylinder. These observations agree well with existing data and findings [1].

**Response amplitude ratio**

The Reynolds effect on the maximum VIV response amplitude ratio was discussed in [1], distinct Re effects between subcritical critical and super-critical Re flow regimes were observed.

Nominal CF VIV amplitude ratios ($A_{nom}/D = \sqrt{2}\sigma_{CF}/D$) of present tests are present in Figure 9, plotting against the reduced velocity at different Re.

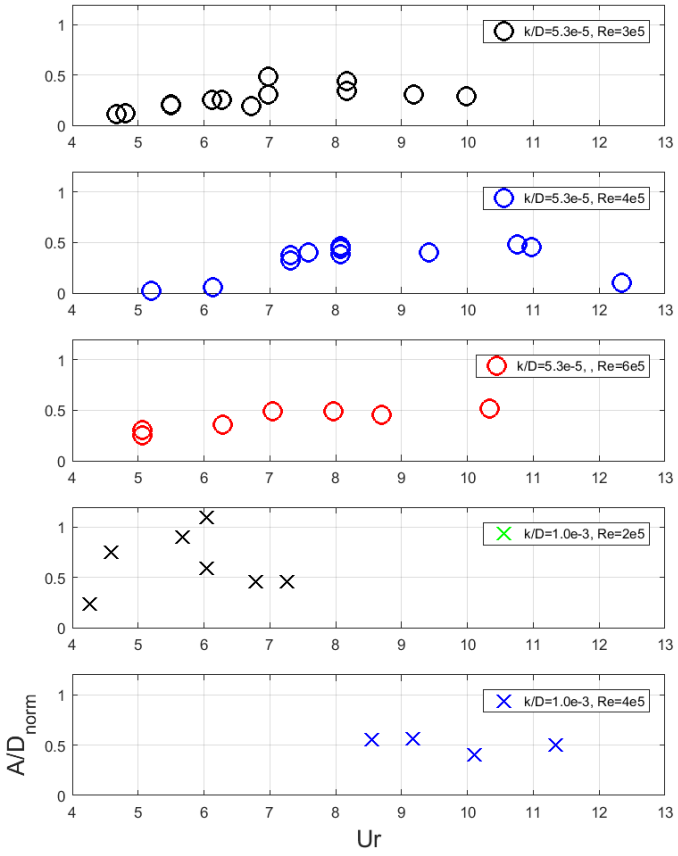


**Figure 9 $A_{nom}/D$ vs. $U_r$ at prototype Re.**

Free oscillation tests on the smooth riser ($k/D = 5.3 \times 10^{-5}$) were performed at three Reynolds numbers: $3 \times 10^5$, $4 \times 10^5$ and $6 \times 10^5$. Among these three sets of free oscillation tests, Re was kept the same for each set by towing the carriage at the same speed. Different reduced velocities were achieved by changing the spring setup. These three Reynolds numbers are within the 'critical' and 'supercritical' flow regimes. It shows the maximum $A_{nom}/D$ is around 0.5 for all three Re numbers. It implies that for a smooth riser, at critical and supercritical flow regime, the maximum response amplitude is not sensitive to Re.

Free oscillation tests on the rough riser ($k/D = 1.0 \times 10^{-3}$) were performed at two Reynolds numbers: $2 \times 10^5$ and $4 \times 10^5$. At $Re = 2 \times 10^5$ (subcritical flow regime), maximum $A_{nom}/D$ is around 1.1, the corresponding $U_r$ is around 6. At $Re = 4 \times 10^5$ (critical flow regime), maximum $A_{nom}/D$ is around 0.56, the corresponding reduced velocity is around 7.5. The effect of Re on the maximum response amplitude ratio is significant and the trend is very similar for both smooth and rough risers. Further discussion will confirm this.

If we compare the results at the same Re $4 \times 10^5$ for both smooth and rough risers, the maximum $A_{nom}/D$ values are 0.5 and 0.56 respectively, which implies the effect from the surface roughness is not significant at this Reynolds number. Earlier studies also showed that the roughness has limited influence on the VIV response in sub-critical Re range [12]. However, no tests with the rough cylinder were carried out at sub-critical Re range in present test.

One set of free oscillation tests on smooth riser was carried out by using the same spring setup, but towing the carriage with different speeds, in such way, both the Re and reduced velocity will be different from test to test. The results are shown in Figure 10. Note that the Re varies from $1 \times 10^5$ to $2.6 \times 10^5$, which is mainly in the subcritical flow regime. We can see that the maximum $A_{nom}/D$ is around 1.76, which is significant higher than the prototype Re number results. Similar high maximum amplitude ratio was also observed in the previous prototype Re VIV tests [1]. The results from both previous and present tests shows that the rigid smooth riser has much higher amplitude in subcritical flow regime than critical and supercritical flow regime.

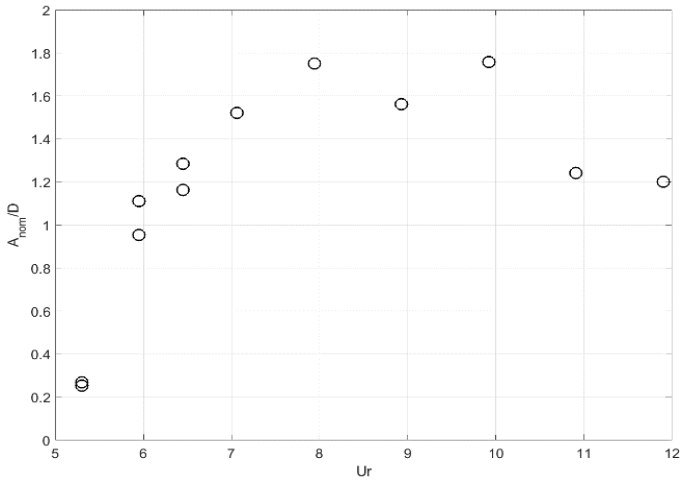


**Figure 10 $A_{nom}/D$ vs. $U_r$ at subcritical Re, for smooth cylinder $k/D = 5.3e-5$.**

The maximum amplitude ratios in CF direction are summarized in Table 3, for both smooth and rough riser models.

Govardhan & Williamson [3] proposed an empirical formula for peak CF response amplitude ratio:

$$A^* = (1 - 1.12 + 0.30\alpha^2)log(0.41Re^{0.36}) \quad (10)$$

where $\alpha$ is a mass-damping parameter, $\alpha = (m^* + C_a)\zeta$. $C_a$ is the potential added mass coefficient, taken as 1.0 for a circular cylinder.

Even this formula is only valid for a range of Re=500-33000 [3], an attempt has been done to show the differences of Re effect

on the peak response amplitude ratio in subcritical and prototype Re. Here we take $\zeta = 0.036$ from Figure 5, which gives $\alpha = 0.0506$.

**Table 3 Maximum amplitude ratio.**

| | $A_{nom,max}/D$ | |
|---|---|---|
| $Re$ | $\frac{\kappa}{D} = 5.3 \times 10^{-5}$ | $\frac{\kappa}{D} = 1.0 \times 10^{-3}$ |
| $1 \times 10^5$ - $2.6 \times 10^5$ | 1.76 | - |
| $2 \times 10^5$ | - | 1.1 |
| $3 \times 10^5$ | 0.49 | - |
| $4 \times 10^5$ | 0.48 | 0.56 |
| $6 \times 10^5$ | 0.49 | - |

The maximum response amplitude ratios in Table 3 are plotted together with the 'Modified Griffin Plot' (defined by formula (10), see Figure 11. It is expected that the results from present experiments do not agree with the 'Modified Griffin plot', due to the Re is out of the valid range of formula (10). But if we take a closer look, at Re around $2 \times 10^5$, the smooth pipe has $A^* = 1.76$, while the rough pipe has $A^* = 1.1$, it is reasonable to believe that the difference is caused by the surface roughness. This Reynolds number is in the TrS0 regime, where the shear layer is fully turbulent, and there is onset of transition from laminar to turbulent at separation point [15]. Larger surface roughness makes this transition occur at a lower Re.

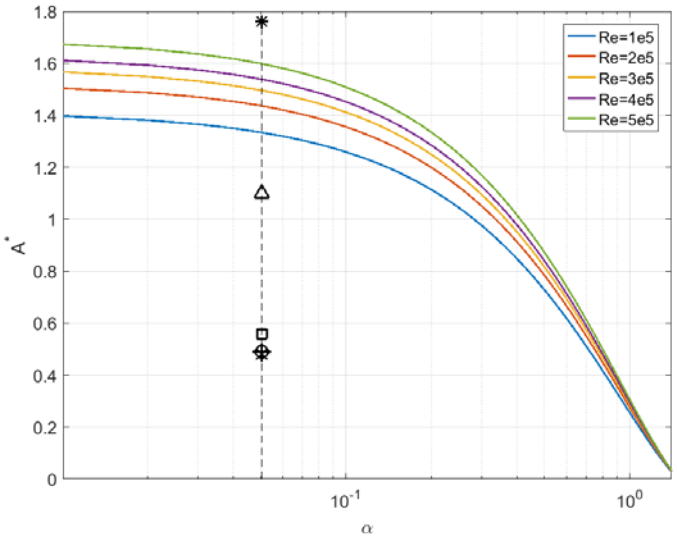


**Figure 11 Calculated peak response amplitude ratio by 'Modified Griffin Plot' [3]. *, $Re = 2.16 \times 10^5$, $k/D = 5.3 \times 10^{-5}$; ○, $Re = 3 \times 10^5$, $k/D = 5.3 \times 10^{-5}$; ×, $Re = 4 \times 10^5$, $k/D = 5.3 \times 10^{-5}$; +, $Re = 6 \times 10^5$, $k/D = 5.3 \times 10^{-5}$; Δ, $Re = 2 \times 10^5$, $k/D = 1.0 \times 10^{-3}$; □, $Re = 4 \times 10^5$, $k/D = 1.0 \times 10^{-3}$.**

Fluctuating lift and drag coefficients were reviewed and presented in Figure 12 by [16]. In TrS0 regime, the lift coefficient decreases dramatically, and this has a direct effect on the $A^*$. The relationship between $A^*$ and lift coefficient is described in [17]:

$$A^* = \frac{C_L}{\frac{8m\zeta\pi^2 St^2}{\rho D^2}} \tag{11}$$

where we can see that under lock-in condition (vortex shedding frequency synchronizes with the cylinder natural frequency), $A^*$ is independent of the flow velocity (Re), but directly influenced by the lift coefficient. What happens if we have a larger surface roughness? As we discussed earlier, it makes this transition occur at lower Re. In other words, at the same Re, the lift coefficient for a rougher cylinder is smaller than that of a smooth cylinder, especially at TrS0 regime. That explains the difference of $A^*$ between a smooth and a rough cylinder.

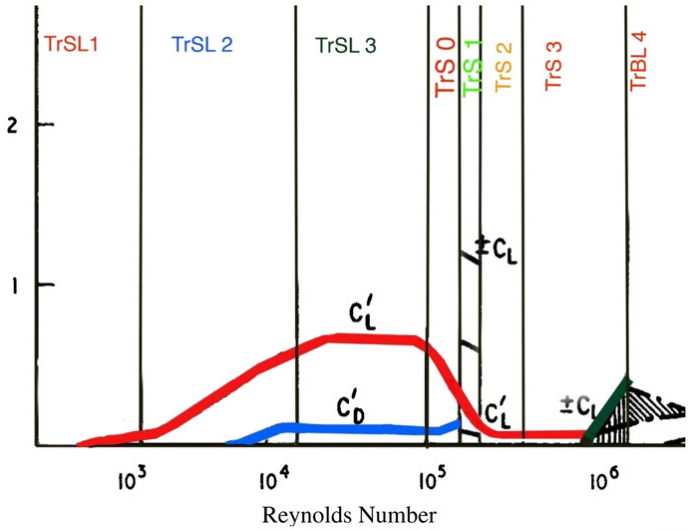


**Figure 12 Fluctuating lift ($C_L'$) and drag ($C_D'$) coefficients, and mean lift ($C_L$) coefficient the TrSL and TrBL regimes [15][16].**

For the three data points with $A^*$ in the range of 0.4 to 0.6, it seems they are neither Re dependent nor sensitive to surface roughness. They have a Re range from $3 \times 10^5$ to $6 \times 10^5$, corresponding to TrS1 to TrS3 regime approximately. In these regimes, the boundary layer transits from laminar to turbulent, and the shear layer is fully turbulent, the surface roughness plays a less important role. The lift coefficient is significantly low and varies little with further increasing Re, so that the $A^*$ is also less sensitive to Re.

**Oscillation frequency**

Figure 13 plots the dominant oscillation frequency against the natural frequency in still water (measured from decay tests in water). It illustrates the difference of added mass in still water and in constant current, The scattering is seen. For a mass-damper-spring system, assuming the damping is small enough to be neglected, $f = \sqrt{k/(m + m_a)}$, the frequency ratio is

$$\frac{f_{osc}}{f_n} = \sqrt{\frac{m+m_{a,n}}{m+m_{a,osc}}} = \sqrt{1 + \frac{m_{a,n}-m_{a,osc}}{m+m_{a,osc}}} \tag{12}$$

where $m_{a,n}$ is the added mass in still water, $m_{a,osc}$ is the added mass when the riser model is freely oscillating.

For the smooth riser model, $f_{osc}/f_n > 1$ at $Re = 3 \times 10^5$, which indicates the oscillating added mass is smaller than the still water added mass; while $f_{osc}/f_n < 1$ at $Re = 4 \times 10^5$ for most of the cases, this is true also for the rough riser model, this indicate the oscillating added mass is larger than the still water added mass.

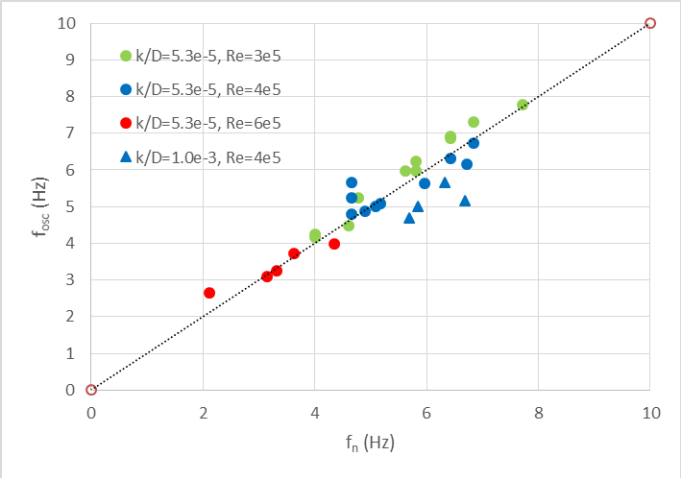


**Figure 13 Oscillation frequency vs. still water natural frequency.**

## Transition

'*Transition*' could happen for elastically supported riser model in constant flow [18]. The transition of the wake induced force will result in different responses, as shown in Figure 14.

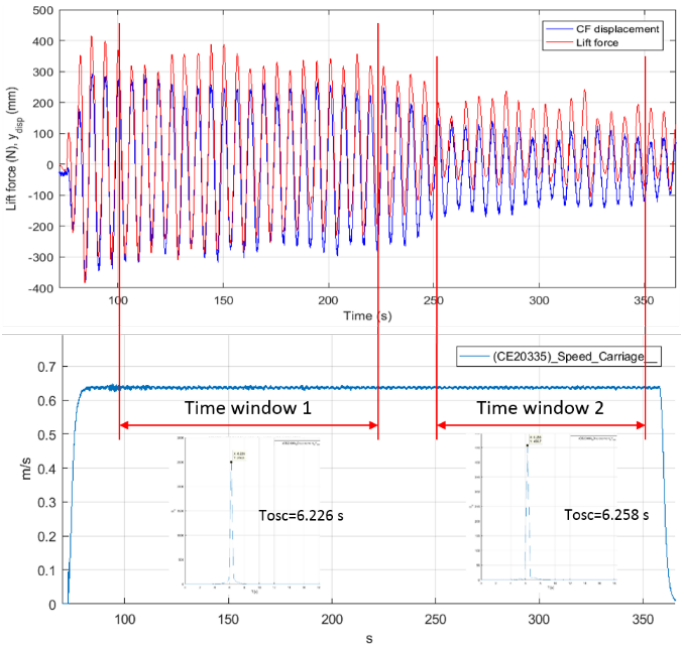


**Figure 14 Free oscillation test on smooth riser, $k/D = 5.3 \times 10^{-5}$, $Re = 3 \times 10^5$, $U_r = 7$. Upper: time histories of lift force and CF response displacement; Lower: time history of towing speed.**

Distinct different response amplitudes are observed in two time-windows, the oscillation periods are slight different. The 'transition' occurred at $t = 250\ s$, the lift force is in phase with the oscillation displacement all the time.

## Excitation coefficient

The excitation coefficients obtained from the forced motion tests are presented as contour plots in Figure 15 and Figure 16. All the forced motion tests were carried out at the same Reynolds number $4 \times 10^5$. Note that in the contour plots, the values of the area without data point are interpolated.

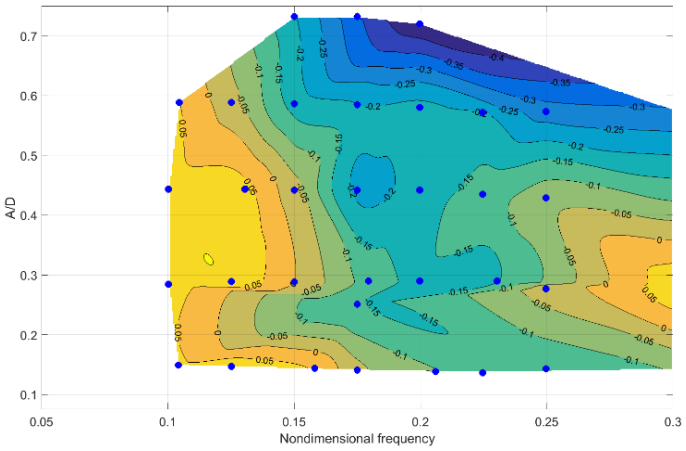


**Figure 15 Plot of contour curves for CF excitation coefficient in an amplitude ratio-nondimensional frequency map, $k/D = 5.3 \times 10^{-5}$, $Re = 4 \times 10^5$. Data points are marked with blue dots.**

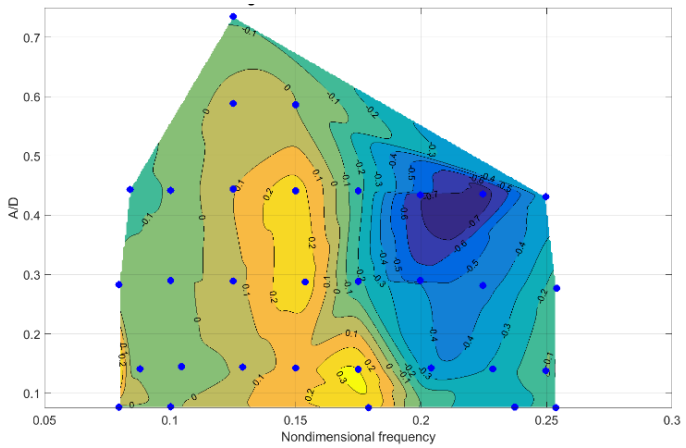


**Figure 16 Plot of contour curves for CF excitation coefficient in an amplitude ratio-nondimensional frequency map, $k/D = 1.0 \times 10^{-3}$, $Re = 4 \times 10^5$. Data points are marked with blue dots.**

In the contour plots, the zero contour lines defines the CF response amplitude for a cylinder without mechanical damping. The areas with positive excitation coefficients are defined as excitation regions, and the zero contour line is the boundary of these regions [19].

From the contour plot of the smooth riser, two excitation regions are clearly seen, one is with $\hat{f}$ from 0.1 to 0.15, the

other is with $\hat{f}$ from 0.275 to 0.3. It also indicates that the excitation region may extend to the non-dimensional frequency lower than 0.1 and higher than 0.3. The maximum amplitude ratio corresponding to zero excitation coefficient is slightly higher than 0.6. This value may change if additional data points are available.

For the riser section with rough surface, calculated excitation coefficients from forced oscillation tests are presented in Figure 16. Positive excitation coefficients for the rough riser section are seen at non-dimensional frequencies 0.125, 0.15 and 0.175. The maximum excitation coefficients is around 0.3 at $\hat{f} = 0.175$. The non-dimensional frequency ranges from 0.11 to 0.19 in the excitation region. The maximum amplitude ratio with zero excitation coefficient is around 0.65. For the $\hat{f}$ larger than 0.25, it is unknown whether there exist another excitation region. For the $\hat{f}$ lower than 0.09, there exists are tiny excitation region, with very large uncertain due to lack of data points.

In present model tests, the rough riser model has a surface roughness ratio $k/D = 1.0 \times 10^{-3}$, which is half of one model of [6], so the results should be comparable. The comparison is summarized in Table 4. In general, results from present study have similar trend and the excitation coefficients have same level of magnitude.

**Table 4 Comparison of excitation coefficients for rough riser.**

| Property. | Present rough riser | ExxonMobil [3] |
|---|---|---|
| $k/D$ | $1.0 \times 10^{-3}$ | $2.0 \times 10^{-3}$ |
| Excitation region | $\hat{f}$: 0.11-0.195 | $U_r$: 2.5-9.5 |
| $A_{CF,max}\|_{C_e=0}/D$ | 0.65 | 0.85 |
| $C_{e,CF,max}$ | $\geq 0.3$ | $\geq 0.5$ |

The differences between present tests and [6] may be attributed to several aspects:

1.Present test has a fixed Re, while ExxonMobile has a varying Re.

2. The surface roughness ratio is not exactly the same between present and ExxonMobil tests.

3. Present full scale riser model was located vertically on the test rig, while ExxonMobil had a horizontal cylinder model.

4. The excitation forces were extracted in different ways.

5. The $L/D$ is around 6 in present tests, ExxonMobil has $L/D$ of 18.

The drag coefficients of all the forced motion VIV tests are plotted against the amplitude ratio, which is shown in Figure 17. Note that the amplitude ratio is the actual measured value instead of defined value. For the smooth riser, the drag coefficient varies from 0.4 to 1.1. While for the rough riser, the drag coefficient ranges between 0.85 and 1.3, which is significantly larger than the smooth riser. At this Reynolds number the fixed smooth riser model has a drag coefficient around 0.4, and the fixed rough riser model has a drag coefficient about 0.95, see Figure 7. The drag amplification due to CF motion is seen, as the amplitude increases, this amplification becomes stronger.

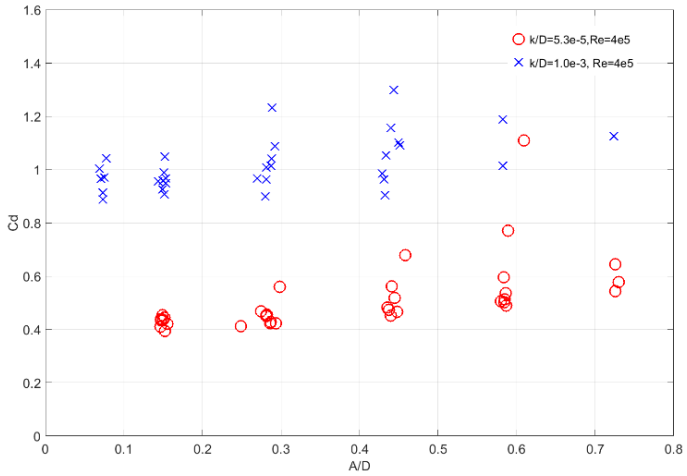


**Figure 17 Drag coefficients of all forced motion VIV tests.**

## CONCLUSIONS

This paper presents some key results of the prototype Re VIV model tests that carried out at MARINTEK. Stationary towing tests, free oscillation VIV tests and forced motion VIV tests on the two full scale rigid riser sections were conducted.

Drag coefficients of 'fixed' riser sections are extracted from stationary tests. Surface roughness effect on the drag coefficient is clearly seen, and the drag crisis is captured for both riser sections. It might be of interest to do more stationary test with even higher Reynolds number, and different surface roughness ratios in order to get more complete data base.

Pure CF free oscillation VIV tests in present study were carried out at fixed Reynolds numbers, different reduced velocities were achieved by adjust the location and arm length of three sets of springs. The key results are the response amplitude ratio. For either smooth or rough riser model in present study, at critical and supercritical flow regimes, the displacement amplitude ratio is not sensitive to Re. However, in subcritical flow regime, the response amplitude ratio is significantly larger than that in at critical and supercritical flow regimes. At a supercritical Reynolds number $4 \times 10^5$, the surface roughness effect on the maximum displacement amplitude ratio is not distinct.

Forced oscillation VIV tests were carried out on both riser section models at a Reynolds number $4 \times 10^5$. The most important results are the excitation coefficients at prototype Reynolds number. Two excitation regions for the 'smooth riser' and one excitation region for the 'rough riser' are identified.

The excitation coefficient at supercritical Re in present study is significantly lower than the excitation coefficients in subcritical flow. Partly due to insufficient data. The excitation region is also different, especially for the riser with rough surface. Amplified drag coefficients are also extracted from forced oscillation VIV tests. Generally, results from present study show similar trends as the literatures.

## ACKNOWLEDGMENTS

The authors gratefully acknowledge Norwegian Deepwater Programme and Statoil for permission to publish these results.

## REFERENCES

[1] Yin, D., Wu, J., Lie, H., Baarholm, R., and Larsen, C. M., “VIV prediction of steel catenary riser - A Reynolds number sensitivity study,” in Proceedings of the Twenty-fifth (2015) International Ocean and Polar Engineering Conference, vol. 3, pp. 1018–1027, 2015.

[2] Klamo, J. T., Leonard, A. & Roshko, A. 2005. On the maximum amplitude for a freely vibrating cylinder in cross-flow. J. Fluids Struct. 21, 429–434.

[3] Govardhan, R.N. & Williamson, C.H.K., 2006, Defining the Modified Griffin Plot in Vortex-Induced Vibration: Revealing the Effect of Reynolds Number Using Controlled Damping, Journal of Fluid Mechanics 561, 147-180.

[4] Swithenbank SB, Vandiver J, Larsen C, Lie H. Reynolds Number Dependence of Flexible Cylinder VIV Response Data. ASME. International Conference on Offshore Mechanics and Arctic Engineering, OMAE2008-57045.

[5] Resvanis TL, Jhingran V, Vandiver J, Liapis S. Reynolds Number Effects on the Vortex-Induced Vibration of Flexible Marine Risers. ASME. International Conference on Offshore Mechanics and Arctic Engineering, OMAE2012-83565.

[6] Ding, Z. J., Balasubramanian, S., Lokken, R. T. and Yung, T.-W., 2004, “Lift and Damping Characteristics of Bare and Straked Cylinders at Riser Scale Reynolds Numbers”, Proceedings of Offshore Technology Conference, Paper No. OTC 16341, Houston, Texas.

[7] Dahl, J. M., Hover, F. S., Triantafyllou, M. S., and Oakley, O. H., “Dual resonance in vortex inducedvibrations at subcritical and supercritical Reynolds numbers,” Journal of Fluid Mechanics, vol. 643, pp. 395–424, 2010.

[8] Lie, H., Braaten, H., Szwalek, J., Massimiliano, R. and Baarholm R. J., "Drilling riser VIV tests with prototype Reynolds numbers". Proceedings of the ASME 32nd International Conference on Ocean, Offshore and Arctic Engineering, Paper No. OMAE2013-11643.

[9] Yin, D. (2013): "Experimental and Numerical Analysis of Combined In-line and Cross-flow Vertex Induced Vibrations". Department of Marine Technology, Norwegian University of Science and Technology. Trondheim, Norway.

[10] Passano, E., Larsen, C. M., Lie, H., and Wu, J. "VIVANA Theory Manual Version 4.6", MARINTEK report MT2014-F135, Trondheim, Norway, June 2016.

[11] Newman, J.N. 1977 Marine Hydrodynamics. MIT Press.

[12] Bridge, C., Willis, N., Sworn, A. and Wilde, J. de. “Development of SHEAR 7 Lift Curves For VIV Analysis And Application To Single Pipe And Bundle Risers,” in Offshore Technology Conference, 2005. OTC-17533.

[13] Miller, B. The Hydrodynamic Drag of Roughened Circular Cylinders National Maritime Institute (Feltham), 1976.

[14] Hoerner, S. F. Fuild-Dynamic Drag 1965.

[15] Zdravkovich, M.M., 1997. Flow Around Circular Cylinders Volume1:Fundamentals. Oxford Science Publications.

[16] Raghavan, K. & Bernitsas, M. M. Experimental investigation of Reynolds number effect on vortex induced vibartion of rigid circular cylinder on elasstic supports Ocean Engineering, 2011, 38, 719-731

[17] Blevins, R. D. 1990 Flow-Induced Vibration, 2nd edition. New York: Van Nostrand Reinhold.

[18] Carberry J, Sheridan J, Rockwell D. "Controlled oscillations of a cylinder: forces and wake modes". J Fluid Mech 2005; 538: 31-69.

[19] Aronsen, K.H. (2007): "An Experimental Investigation of In-line and Combined In-line and Cross-flow Vertex Induced Vibrations". Department of Marine Technology, Norwegian University of Science and Technology. Trondheim, Norway.